Full Counting Statistics and Phase Diagram of a Dissipative Rydberg Gas

N. Malossi,[1,2] M. M. Valado,[1,2] S. Scotto,[2] P. Huillery,[3] P. Pillet,[3] D. Ciampini,[1,2,4] E. Arimondo,[1,2,4] and O. Morsch[1,2]
[1]*INO-CNR, Via G. Moruzzi 1, 56124 Pisa, Italy*
[2]*Dipartimento di Fisica "E. Fermi," Università di Pisa, Largo Pontecorvo 3, 56127 Pisa, Italy*
[3]*Laboratoire Aimé Cotton, CNRS, Univ Paris-Sud 11, ENS-Cachan, Campus d'Orsay Batiment 505, 91405 Orsay, France*
[4]*CNISM UdR Dipartimento di Fisica "E. Fermi," Università di Pisa, Largo Pontecorvo 3, 56127 Pisa, Italy*
(Received 18 September 2013; published 8 July 2014)

Ultracold gases excited to strongly interacting Rydberg states are a promising system for quantum simulations of many-body systems. For off-resonant excitation of such systems in the dissipative regime, highly correlated many-body states exhibiting, among other characteristics, intermittency and multimodal counting distributions are expected to be created. Here we report on the realization of a dissipative gas of rubidium Rydberg atoms and on the measurement of its full counting statistics and phase diagram for both resonant and off-resonant excitation. We find strongly bimodal counting distributions in the off-resonant regime that are compatible with intermittency due to the coexistence of dynamical phases. Our results pave the way towards detailed studies of many-body effects in Rydberg gases.

DOI: 10.1103/PhysRevLett.113.023006 PACS numbers: 32.80.Ee, 05.70.Fh, 34.20.Cf

Ultracold atoms excited to high-lying Rydberg states [1] have been shown in recent years to be promising candidates for experimental implementations of quantum computation and quantum simulation [2–4]. The strong and controllable interactions between Rydberg atoms mean that fast two-qubit quantum gates and models of many-body Hamiltonians can, in principle, be efficiently realized. As a further important ingredient, dissipation has been shown to lead to novel phases [5–8] and to facilitate, under certain conditions, the creation of pure and coherent many-body states [9–11] and quantum simulations [2,3].

Thus far, Rydberg excitations in cold gases have been studied almost exclusively in the resonant, nondissipative regime. In those experiments the strong interactions between Rydberg atoms manifest themselves either as spatial correlations [12,13] or through a reduction of fluctuations [14]. In this Letter we show that for off-resonant excitation the behavior of the system depends strongly on the detuning and the sign of the interaction. We characterize our system through the full counting statistics of the excitation events, similarly to the methods recently used in condensed matter physics to unveil correlations in electronic transport processes [15,16]. In the dissipative regime, we observe strongly bimodal counting distributions [5,7,8], indicating intermittency and/or phase coexistence, as predicted in [5,7], or bistability, as observed in [17].

Our experiments are performed using 87-rubidium atoms in magneto-optical traps that are excited to $70S$ Rydberg states using a two-photon excitation process with detuning Δ from resonance and two-photon Rabi frequencies of up to 400 kHz (see Ref. [14] for details). The first step laser at 420 nm is detuned by 2 GHz from the intermediate $6P$ state to ensure that the latter is not populated on the time scale of the experiment. The second step laser at 1013 nm is focused to a waist of 80 μm, and the waist of the first step laser can be varied between 6 and 40 μm, allowing us to change the overlap between the atomic clouds of size $\approx$30–100 μm [with peak densities around $(0.9\text{–}5) \times 10^{11}$ cm^{-3}] and the excitation lasers, and hence the effective excitation volume, which ranges from $\approx 10^{-7}$ to $\approx 5 \times 10^{-6}$ cm^3. The smallest waist of the first step laser is then smaller than the blockade radius and hence the excitation geometry is quasi-one-dimensional. After the excitation pulse, during which the magneto-optical trap laser beams are switched off, the Rydberg atoms are field ionized and detected using a channeltron charge multiplier, whose output is recorded on an oscilloscope [see Fig. 1(a)]. The full counting distributions were obtained by performing 500 repetitions of the experiment. The overall Rydberg detection efficiency $\eta \approx 40\%$ was taken into account in calculating the observed counting distributions $(P(x))_{\mathrm{obs}}$ for the number x of Rydberg excitations and their central moments from the actual distributions $P(x)$ (see Supplemental Material [18] and definitions below), extending the treatment of [19] to higher moments.

Figures 1(b)–1(d) illustrate the different excitation regimes. Away from resonance [Fig. 1(d)], two atoms at a distance r from each other can undergo a pair excitation if $C_6/r^6 = 2\hbar\Delta$, where C_6 is the van der Waals coefficient. For the $70S$ Rydberg state in 87-Rb, $C_6 = h \times 1.2\,\mathrm{THz}\mu\mathrm{m}^6$, so $r = 6.26 \pm 0.1$ μm for a typical detuning of 10 MHz (the range in r is due to the finite laser linewidth of about 0.5 MHz). This resonant condition is the opposite of the blockade effect [Fig. 1(c)] [20], where the interaction *suppresses* excitations, allowing at most one single (collective) excitation within a blockade radius. The time scale for off-resonant pair excitations can be estimated from the two-photon Rabi frequency $\Omega_{\mathrm{off}} = \Omega^2/(2\Delta)$. In our

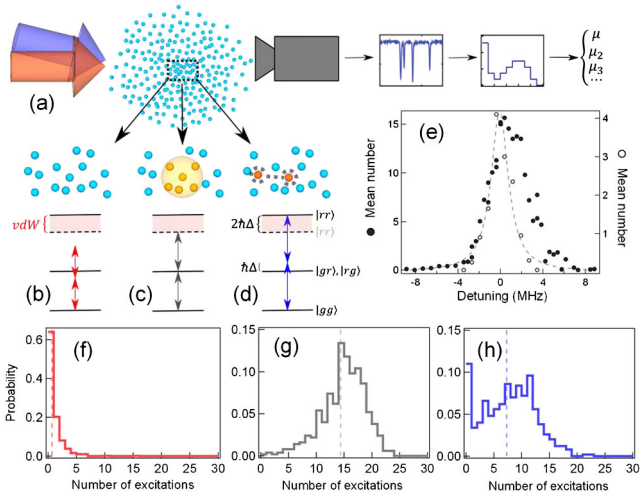

FIG. 1 (color online). (a) Schematic representation of the experimental procedure. (b)–(d) Resonant and off-resonant excitation processes for interacting Rydberg atoms. (vdW indicates the energy shift due to the van-der-Waals interaction). (e) Mean number of Rydberg excitations as a function of detuning. Here and throughout the Letter we omit the subscript "obs" indicating the observed quantities. The excitation durations are 1 μs (gray symbols, right-hand vertical axis) and 20 μs (black symbols, left-hand vertical axis). (f)–(h) Histograms of the counting distributions in the resonant and off-resonant regimes. The detunings are $\Delta/2\pi = -3.5$ MHz (f), $\Delta/2\pi = 0$ (g), and $\Delta/2\pi = +3.5$ MHz (h). The dashed vertical lines indicate the mean number of excitations. The Rabi frequency is $2\pi \times 400$ kHz, the interaction volume 10^{-7} cm^3, and the density 1.8×10^{11} cm^{-3}.

experiment, $\Omega \approx 2\pi \times 200$ kHz, so for $\Delta/2\pi = 2$ MHz, we have $\Omega_{\text{off}} \approx 2\pi \times 10$ kHz, which is much smaller than the collective Rabi frequency $\Omega_{\text{coll}} \approx 2\pi \times 1.4$ MHz (for a number $N_{db} \approx 50$ of atoms inside a blockade volume [1,21]). Also, excitations of atoms at a distance r_c from an already excited atom satisfying $C_6/r_c^6 = \hbar\Delta$ are possible. Finally, for a detuning with opposite sign, neither single-particle nor pair excitations are resonant, leading to an overall suppression of the excitation probability [Fig. 1(b)].

Figure 1(e) shows the mean number of Rydberg excitations as a function of detuning for two different excitation durations. For the 1 μs pulse off-resonant pair excitations are negligible and, hence, the line shape is symmetric. For a 20 μs pulse, however, the excitation time approaches $2\pi/\Omega_{\text{off}} \approx 100$ μs, and off-resonant excitations become visible, resulting in an asymmetric line shape (on these time scales, excitations mediated by already excited atoms are also likely to occur and may dominate the dynamics in our experiments). Further evidence for the different excitation regimes is found in the histograms of the counting distributions [Figs. 1(f)–1(h)]. On resonance, the distribution is roughly Poissonian [it becomes sub-Poissonian in the fully blockaded regime, as seen in Fig. 3(b)], whereas for positive detuning it becomes multimodal. For negative detuning, the histogram confirms the expected strong suppression of excitations.

We now turn to the dissipative off-resonant excitation regime, in which several excitation-spontaneous emission cycles occur during the excitation pulse (in this regime thermal motion and the forces between excited atoms can lead to a motion of the atoms of several tens of microns). Even though our experimental system does not allow us to work in the fully coherent regime (due to limitations in the laser linewidth and power), the 20 μs excitation duration in Fig. 1 is an order of magnitude shorter than the lifetime of the 70S Rydberg state of around 200 μs. Comparing the counting distributions for different durations (Fig. 2), in which the Rabi frequency was adjusted in order to keep the mean value constant, we find that the bimodality increases for longer times, suggesting that dissipation favors bimodality (as theoretically predicted in Refs. [5–7]). This is confirmed by the increase in the bimodality parameter with excitation duration (inset of Fig. 2).

The complete counting distribution provides more insight into the properties of our system (as in, e.g., Ref. [22] for the phase transition of a spin-1 Ising model). We have characterized the full counting statistics of $P(x)$ over a range of Rabi frequencies (see Fig. 3) by analyzing the nth order central moments $\mu_n = \langle (x - \bar{x})^n \rangle$ up to $n = 4$ as well as their associated normalized quantities Mandel Q factor $Q = \mu_2/\bar{x} - 1$, skewness $\gamma = \mu_3/\mu_2^{3/2}$, Binder cumulant $B = 1 - \mu_4/(3\mu_2^2)$, and bimodality coefficient $b = (\gamma^2 + 1)/(\mu_4/\mu_2^2)$ as a function of the mean number $\bar{x}$. We compare our experimental results to three simple models in order to highlight the main features: a perfectly monomodal model with mean $\bar{x}$ and central moments $\mu_{2,3,4,\ldots} = 0$, a Poissonian monomodal model with $\mu_2 = \mu_3 = \bar{x}$ and $\mu_4 = \bar{x}(1 + 3\bar{x})$, as well as a bimodal model consisting of two modes at x_1 and x_2 with probabilities

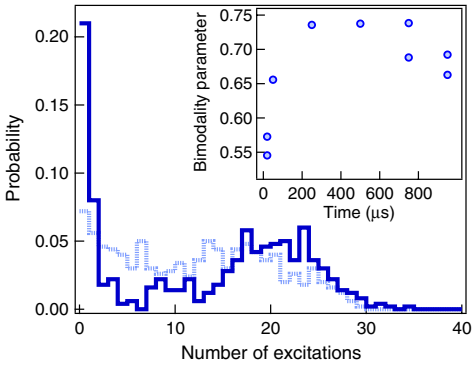

FIG. 2 (color online). Experimental results showing the crossover to the dissipative regime in off-resonant excitation ($\Delta = 11.5$ MHz). As the duration of the excitation is increased from 20 μs (dotted line) to 950 μs (solid line), the counting distributions become more strongly bimodal. The inset shows the bimodality parameter as a function of the excitation duration.

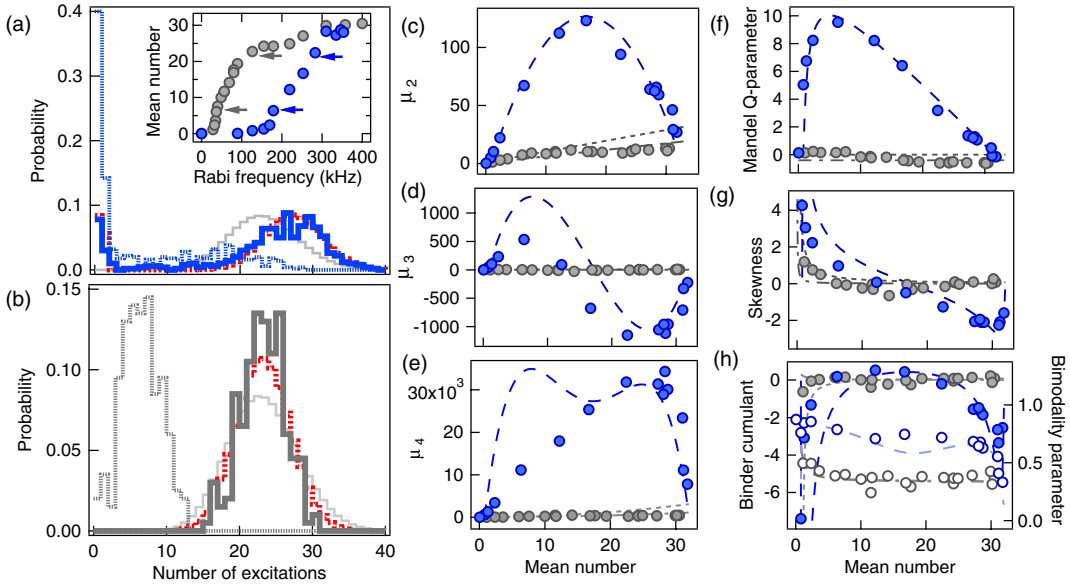

FIG. 3 (color online). (a) Off-resonant ($\Delta/2\pi = 11.5$ MHz) and (b) resonant counting distributions in the dissipative regime, for equal mean numbers 6 (dashed lines) and 23 (solid lines), respectively [indicated by the arrows in the inset of (a), which shows the mean number of excitations as a function of the Rabi frequency]. The dotted red lines are the results of the bimodal model in (a) and the perfectly monomodal model in (b), whereas the solid light gray lines show the distributions expected for Poissonian distribution with the same mean values. (c)–(e) The second, third, and fourth central moments of the off-resonant (blue) and on-resonant (gray) counting distributions. Panels (f)–(h) show the associated normalized quantities (see text). The lines in (c)–(h) are the results of the simple bimodal (dashed, with $x_1 = 1$ and $x_2 = 65$), Poissonian monomodal (dotted), and perfectly monomodal (dot-dashed) models. The detection efficiency of 40% was taken into account. For the bimodal model, the theoretical values were scaled by a factor of ≈0.5 in order to facilitate a qualitative comparison with the experimental data. The interaction volume is 3.6×10^{-6} cm^3, the density 1×10^{11} cm^{-3}, and the excitation duration 950 μs.

$1-\alpha$ and α, for which $\bar{x} = (1-\alpha)x_1 + \alpha x_2$ and $\mu_n = (1-\alpha)(x_1 - \bar{x})^n + \alpha(x_2 - \bar{x})^n$.

Figures 3(a) and 3(b) show the off- and on-resonant counting distributions for two mean values (the same in both graphs), illustrating the bimodality for off-resonant excitation and the sub-Poissonian character of the distribution on resonance. This difference is clearly seen in the dependence of μ_2 and the Mandel Q factor on the mean number: On resonance those quantities are consistent with Poissonian distributions for small mean numbers but become increasingly sub-Poissonian for larger numbers. By contrast, in the off-resonant case μ_2 initially *increases*, reaching a peak at about half the maximum number of excitations (the Q factor peaks at smaller mean numbers due to its normalization), which is determined by the ratio between the cloud volume and the volumes associated with the blockade radius and the resonant distance, respectively. The peak in μ_2 can be interpreted as a signature of a dynamical phase transition (see below) for which, in a two-well phase model, μ_2 (i.e., the susceptibility) has a maximum. As can be seen in Figs. 3(c)–3(h), the results of the off-resonant case are in qualitative agreement with a simple bimodal model. In particular, the bimodality coefficient [Fig. 3(h)] off resonance is consistently higher (0.7–0.8) than for the resonant case (around 0.4), emphasizing the qualitative difference between the two regimes. Whereas the agreement is excellent for μ_2, it is less good for the higher central moments, which indicates that the simple model used here needs to be refined to explain the behaviour of our system. Also, particularly for higher moments the detection efficiency η (which may be a function of the ion number itself) sensitively influences the observed behavior.

The results shown in Fig. 3 can be interpreted in terms of a dynamical phase transition between a paramagnetic and an antiferromagnetic phase in a (finite-size) dissipative Ising model with a transverse field, as shown in Refs. [5,7]. Although in those works the atoms are assumed to be arranged in a crystalline structure, the distance-selective resonance mechanism described above means that in our experiment the Rydberg excitations should arrange themselves in a regular array [23]. In Fig. 4 we show a phase diagram for our system. The mean Rydberg number (analogous to the magnetization in the Ising model) as a function of the Rabi frequency exhibits a smooth crossover between 0 excitations and a maximum number of around 30 [see also Fig. 3(a)], with the position of the crossover depending on the detuning. This is expected from the analogy with an Ising spin system [24], where the critical value of the transverse field (the Rabi frequency in our system) increases with increasing Ising interaction (the detuning in our case). Moreover, the distinct peak in the

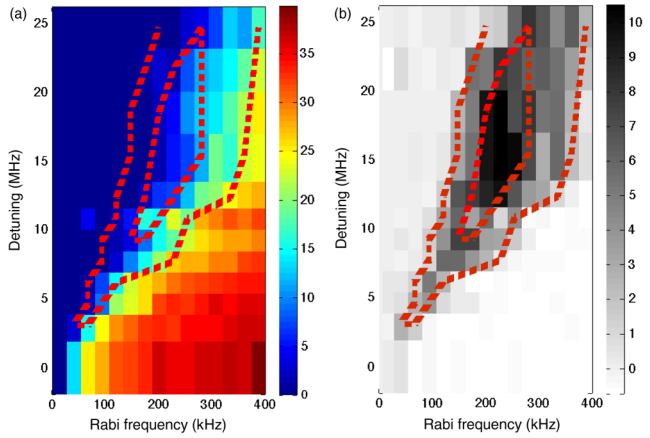

FIG. 4 (color online). Phase diagram in the dissipative regime. Panel (a) shows the mean number of Rydberg excitations and (b) the Mandel Q factor as a function of Rabi frequency and detuning. In (a) and (b) the red dashed lines indicate the transition to $Q > 1$ and $Q > 7$. The interaction volume is 3×10^{-7} cm^3 and the density 1.6×10^{11} cm^{-3}.

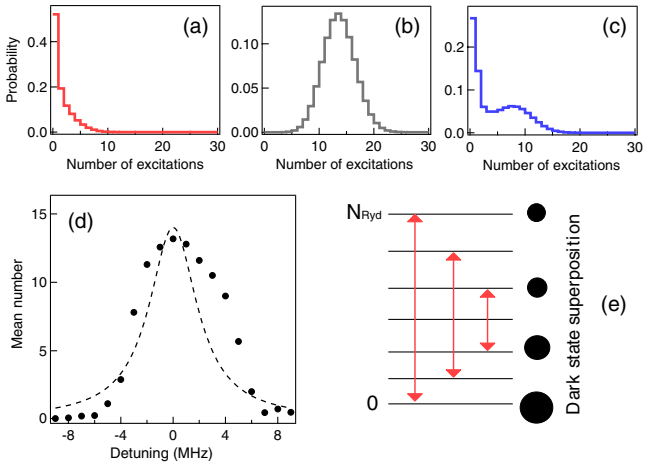

FIG. 5 (color online). (a)–(c) Numerical simulations of the counting distributions for $\Delta/2\pi = -5, 0, 5$ MHz, respectively. The finite detection efficiency is taken into account through a convolution with a binomial function. In (d) the mean values are plotted as a function of detuning. Comparison with a Lorentzian fit (dashed line) centered at $\Delta = 0$ highlights the asymmetry of the line shape (simulation parameters: Rabi frequency 130 kHz, excitation duration 4 μs, density 9×10^{10} cm^{-3}, and interaction volume 8.9×10^{-8} cm^3). (e) Energy levels in the Dicke model of Rydberg excitations (for $\Delta > 0$). The laser excitation is blocked at the state N_{Ryd} within a dark state superposition unbalanced towards the ground state (schematically represented here for the case $N_{\mathrm{Ryd}} = 6$). In the mean-field approximation, the resonance condition $W_{ss}^{(N_{\mathrm{Ryd}}/2)+1} - W_{ss}^{(N_{\mathrm{Ryd}}/2)-1} = \hbar\Delta$ leads to several multiphoton resonances between the intermediate Dicke states. Those excitations produce multilambda-level configurations within the $0 \rightarrow N_{\mathrm{Ryd}}$ ladder.

Mandel Q factor (and hence in μ_2, which corresponds to the susceptibility) in the transition region is compatible with the predicted intermittent behavior of the system [5,7] (as evidenced by the bimodal counting distributions in that region) due to the coexistence of active and inactive phases. In order to prove that interpretation directly, however, it will be necessary to observe the time evolution of a single experimental realization, e.g., through the observation of photons emitted during the decay process [17]. In principle, the full counting statistics obtained in our experiments allows us to determine the critical exponents of the phase transition, e.g., by changing the system size and looking for data collapse of the Binder cumulant [25].

Finally, we present the results of a numerical simulation [Figs. 2(a)–2(d)] based on an extension of the Dicke model applied to Rydberg excitations [14,26] (see the Supplemental Material [18]) that is valid at interaction times shorter than those corresponding to the atomic decoherence mechanisms and reproduces the main features observed in the experiment. Briefly, the original Dicke model was modified by including the van der Waals interactions between the collective Dicke states (taking into account the R^{-3} contribution at short distances for S states) that contain the full statistical information about the collective Rydberg excitation. The laser acting on the cold atoms initially produces a number of Rydberg excitations through a coherent mechanism as for a gas of noninteracting particles. When this number reaches an upper limit [see Fig. 5(e)], the interactions in the systems cause the excitations to be transferred towards an incoherent mixture of states, which results in a sum of a coherent superposition of quantum states (pure density matrix) and an incoherent mixture of occupation probabilities (impure density matrix). This peculiar quantum state is, to the best of our knowledge, an original result of our investigation. The projective quantum measurement of the number of Rydberg excitations, finally, leads to the bimodal counting distributions. Whereas the model is not expected to give quantitative agreement with the experiment (as it does not, for instance, take into account the spatial inhomogeneity of the cloud, the residual velocity of the atoms, or decay from the Rydberg state), for reasonable choices of the parameters in the simulation the qualitative agreement of Figs. 5(a)–5(d) with the experimental data of Fig. 1 is good.

In conclusion, we have analyzed resonant and off-resonant Rydberg excitations in a cold rubidium gas in the dissipative regime through full counting statistics. We have shown that the full counting statistics reveals characteristic features of the system that are not evident in the mean or standard deviation typically measured in such experiments. Our technique should be useful for the characterization of Rydberg excitations in optical lattices [27] in which, e.g., the Ising model can be realized, and in experiments with chirped excitation lasers aimed at the adiabatic creation of Rydberg crystals [28–30]. More generally, the full counting statistics will be an important

tool for unveiling many-body effects in Rydberg excitations [31].

This work was supported by PRIN and the EU Marie Curie ITN COHERENCE. The authors thank R. Fazio, A. Tomadin, M. Dell'Orso, R. Mannella, and I. Lesanovsky for discussions.

[1] D. Comparat and P. Pillet, J. Opt. Soc. Am. B **27**, A208 (2010).
[2] F. Verstraete, M. M. Wolf, and J. I. Cirac, Nat. Phys. **5**, 633 (2009).
[3] H. Weimer, M. M. ller, I. Lesanovsky, P. Zoller, and H. P. Büchler, Nat. Phys. **6**, 382 (2010).
[4] M. Saffman, T. G. Walker, and K. Mølmer, Rev. Mod. Phys. **82**, 2313 (2010).
[5] C. Ates, B. Olmos, J. P. Garrahan, and I. Lesanovsky, Phys. Rev. A **85**, 043620 (2012).
[6] T. E. Lee, H. Häffner, and M. C. Cross, Phys. Rev. A **84**, 031402(R) (2011).
[7] T. E. Lee, H. Häffner, and M. C. Cross, Phys. Rev. Lett. **108**, 023602 (2012).
[8] A. Hu, T. E. Lee, and C. W. Clark, Phys. Rev. A **88**, 053627 (2013).
[9] E. M. Kessler, G. Giedke, A. Imamoglu, S. F. Yelin, M. D. Lukin, and J. I. Cirac, Phys. Rev. A **86**, 012116 (2012).
[10] S. Diehl, A. Tomadin, A. Micheli, R. Fazio, and P. Zoller, Phys. Rev. Lett. **105**, 015702 (2010).
[11] H. Schwager, J. I. Cirac, and G. Giedke, Phys. Rev. A **87**, 022110 (2013).
[12] A. Schwarzkopf, R. E. Sapiro, and G. Raithel, Phys. Rev. Lett. **107**, 103001 (2011).
[13] P. Schauß, M. Cheneau, M. Endres, T.i Fukuhara, S. Hild, A. Omran, T. Pohl, C. Gross, S. Kuhr, and I. Bloch, Nature (London) **491**, 87 (2012).
[14] M. Viteau, P. Huillery, M. G. Bason, N. Malossi, D. Ciampini, O. Morsch, E. Arimondo, D. Comparat, and P. Pillet, Phys. Rev. Lett. **109**, 053002 (2012).
[15] A. Braggio, J. König, and R. Fazio, Phys. Rev. Lett. **96**, 026805 (2006).
[16] A. O. Gogolin and A. Komnik, Phys. Rev. Lett. **97**, 016602 (2006).
[17] C. Carr, R. Ritter, C. G. Wade, C. S. Adams, and K. J. Weatherill, Phys. Rev. Lett. **111**, 113901 (2013).
[18] See Supplemental Material at http://link.aps.org/supplemental/10.1103/PhysRevLett.113.023006 for the mathematical treatment of the detection efficiency and a many-body Dicke model of Rydberg excitations.
[19] J. A. Abate, H. J. Kimble, and L. Mandel, Phys. Rev. A **14**, 788 (1976).
[20] T. Amthor, C. Giese, C. S. Hofmann, and M. Weidemüller, Phys. Rev. Lett. **104**, 013001 (2010).
[21] Y. O. Dudin, L. Li, F. Bariani, and A. Kuzmich, Nat. Phys. **8**, 790 (2012).
[22] S.-H. Tsai and S. R. Salinas, Braz. J. Phys. **28**, 58 (1998).
[23] M. Gärttner, K. P. Heeg, T. Gasenzer, and J. Evers, Phys. Rev. A **88**, 043410 (2013).
[24] H. Weimer, R. Löw, T. Pfau, and H. P. Büchler, Phys. Rev. Lett. **101**, 250601 (2008).
[25] P. Werner, K. Völker, M. Troyer, and S. Chakravarty, Phys. Rev. Lett. **94**, 047201 (2005).
[26] J. Stanojevic, V. Parigi, E. Bimbard, A. Ourjoumtsev, P. Pillet, and P. Grangier, Phys. Rev. A **86** 021403 (2012).
[27] M. Viteau, M. G. Bason, J. Radogostowicz, N. Malossi, D. Ciampini, O. Morsch, and E. Arimondo, Phys. Rev. Lett. **107**, 060402 (2011).
[28] T. Pohl, E. Demler, and M. D. Lukin, Phys. Rev. Lett. **104**, 043002 (2010).
[29] J. Schachenmayer, I. Lesanovsky, A. Micheli, and A. J. Daley, New J. Phys. **12** 103044 (2010).
[30] R. M. W. van Bijnen, S. Smit, K. A. H. van Leeuwen, E. J. D. Vredenbregt, and S. J. J. M. F. Kokkelmans, J. Phys. B **44**, 184008 (2011).
[31] H. Schempp, G. Günter, M. Robert-de-Saint-Vincent, C. S. Hofmann, D. Breyel, A. Komnik, D. W. Schönleber, M. Gärttner, J. Evers, S. Whitlock, and M. Weidemüller, Phys. Rev. Lett. **112**, 013002 (2014).